Weak Lensing with the Very Large Telenscope

M. Lombardi & P. Rosati
European Southern Observatory, Karl-Schwarzschild-Str. 2, D-85748, Garching, Germany

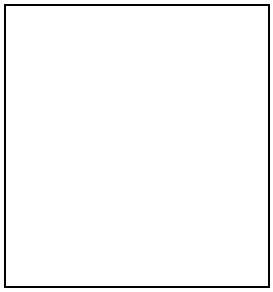

The cluster of galaxies MS1008.1−1224, observed by the VLT Unit 1, provides a unique opportunity to make a detailed weak lensing mass reconstruction. The combination of deep exposure, good seeing, small instrument-induced distortions, and multi-band information allows us to obtain a reliable mass distribution and to study in detail the impact of systematic errors on weak lensing reconstructions. Moreover, the availability of radial velocities for 65 galaxies in MS1008 from the CNOC survey (Carlberg et al. 1996), as well as X-ray spectroscopic observations, provide independent estimates of the total mass. The mass we obtain within $1\,h_{50}^{-1}$ Mpc, $5.3 \times 10^{14}\,h_{50}^{-1}$ $M_\odot$ is in excellent agreement with X-ray estimates.

1 Introduction

The study of the weak lensing distortion of background galaxies is a powerful tool for measuring the mass distribution of galaxy clusters. It has long been recognized (Tyson et al. 1984) that the tidal field of a cluster acts by slightly modifying the images of distant, background galaxies. To date, there are approximately 20 clusters which have been well studied with lensing techniques (see, e.g., Mellier 1998 for a review). In several cases the resulting masses are claimed to be larger (by a factor of two) than those obtained using different methods. At present, it is not known if this discrepancy is due to biases and inaccuracies in the X-ray and dynamical estimates, or to the lensing data reduction method. As a matter of fact, it is not even clear whether there is a real discrepancy (see Wu et al. 1998). For example, Boehringer et al. (1998) have shown that different mass estimators are in excellent agreement when very good quality X-ray and optical data are used.

We present here a detailed weak lensing reconstruction of the cluster MS1008 using Very Large Telenscope (VLT) data. The large surface density of background galaxies in these images, as well as the sharpness of the PSF and its small variations across the field, significantly improve the accuracy in measuring the distorsion field from object ellipticities. As a result, high signal-to-noise shear maps can be obtained. This allows us to better investigate the effect

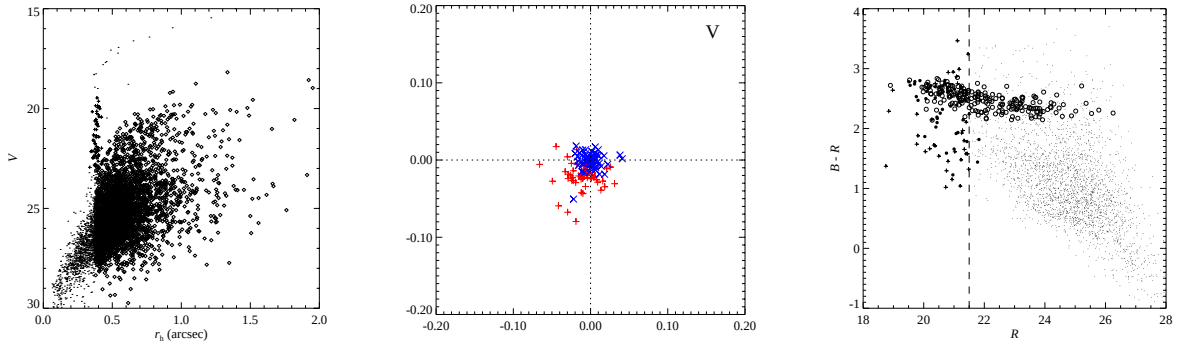

Figure 1: **Left:** The half-light radius vs. magnitude of the objects identified on the V band. **Middle:** The distribution of uncorrected ("plus" signs) and corrected ("multiply" sign) star ellipticities on the complex plane. **Right:** Color-magnitude diagram for the cluster. The open circles are galaxies assumed to belong to the cluster; the filled circles are galaxies with redshift $0.29 < z < 0.32$; dots are the background galaxies.

of systematics involved in the mass inversion procedure, which in this case exceed statistical errors.

In the following we adopt the cosmology $\Omega = 0.3, \Omega_\Lambda = 0.7, H_0 = 50 h_{50}$ km s^{-1} Mpc^{-1}.

2 Weak lensing analysis

For the analysis of the weak lensing signal we mainly used the IMCAT package by Kaiser (Kaiser, Squires, & Broadhurst, 1995) with some refinements described below. A single master catalog was construted by perfoming object detection on the coadded B + V + R + I image. Weak lensing analysis was then carried out *independently* on the four bands. In particular, for each band, we measured object shapes and sizes, and performed star / galaxy separation, PSF correction, and mass reconstruction.

Objects were identified using the IMCAT peak finding algorithm which utilizes a set of images convolved with top-hat filters of different sizes. The local sky level and its gradient were measured for each object by computing the mode of pixels values on a circular annulus around the object's peak. Shape parameters were measured using a Gaussian weight function. The complex ellipticity ϵ was thus calculated from the quadrupole moments Q_{ij} using the definition

$$\epsilon = \epsilon_1 + \mathrm{i}\epsilon_2 = \frac{Q_{11} - Q_{22} + 2\mathrm{i}Q_{12}}{Q_{11} + Q_{22}} \,. \qquad (1)$$

Finally, object detections were visually inspected and residual spurious sources, such as noise, cosmic rays, blends, were removed, and bright stars were masked out.

Star / galaxy classification was performed independently in each of the four images. Relatively bright stars can easily be identified on the half light radius r_h vs. magnitude plot (Fig. 1, left) as a narrow vertical strip, which turns over for saturated stars. The star locus is clearly visible against the distribution of galaxies in the half-light radius r_h vs. magnitude plot down to $V = 23$. Thus, more than 60 high S/N stars across the field of view could be used to model the PSF pattern and to correct galaxy ellipticities (Fig. 1, middle). Objects with $r_\mathrm{h} < r_{\mathrm{stars}}$ are mainly very faint galaxies which we excluded in our analysis, as the errors in the determination of their quadrupole moments are very large.

The deep multicolor photometry provided by the FORS observations, in combination with a large number of spectroscopic redshifts on MS1008 available from the CNOC survey (Yee et al. 1998), allows the cluster galaxies to be effectively separated from the foreground and background galaxy population (see Fig. 1, right).

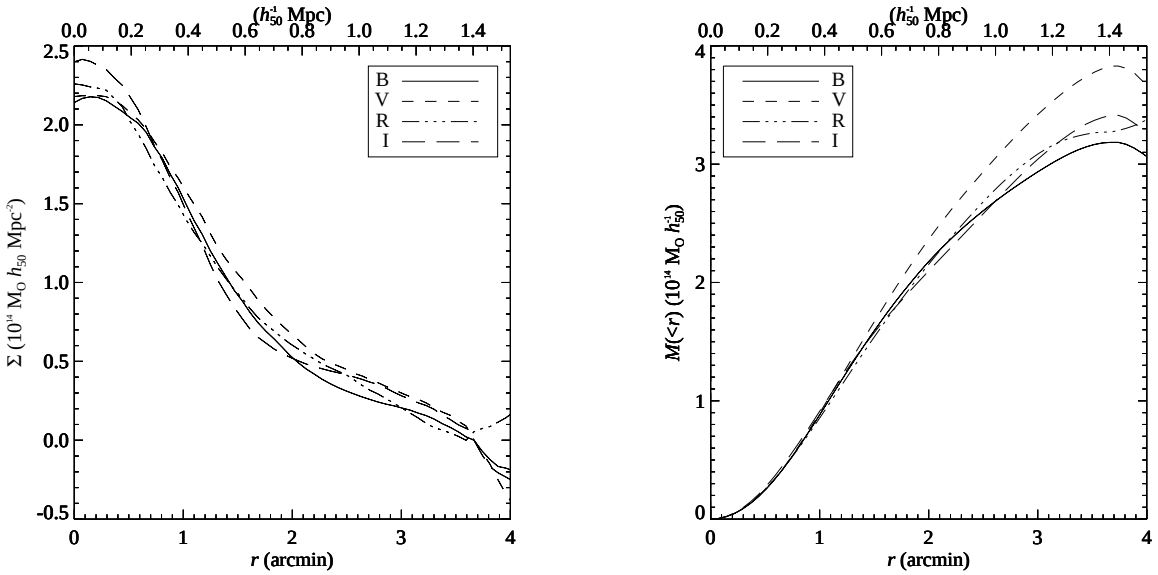

Figure 2: The radial profile (left) and the cumulative radial profile (right) of the mass distributions obtained in the four bands.

The shear map was determined following the method of Luppino & Kaiser (1997; see also Hoekstra et al. 1998), which allows to properly correct for the isotropic and anisotropic part of the PSF, using a set of high S/N stars in the field. Some modifications of this method (Lombardi et al. 2000; Lombardi & Bertin 1999) were used in order to maximize the S/N. For the reconstructions shown below a *Gaussian smoothing function* with scale length $\sigma_W = 30''$ was used; this sets also the scale of the smaller substructure that can be detected in our analysis. In order to convert the dimensionless mass map obtained from weak lensing we need an estimate of the redshift distribution $p(z)$ of the background galaxies. A *statistical* estimate of $p(z)$ was obtained by using the catalogue of photometric redshifts of Fernández-Soto et al. (1999) in the Hubble Deep Field North.

The radial profiles obtained from the two-dimensional mass maps are shown in Fig. 2. The differential radial profiles are in excellent agreement with each other, and their scatter is smaller than 5%. This can also be taken as a roughly estimate of the overall statistical error. The cluster mass as function of radius can be read off the cumulative radial profile in Fig. 2 (right). The larger scatter in this plot is mainly due to the mass sheet degeneracy (Schneider & Seitz, 1995), which was removed by assuming that the cluster mass goes to zero at large radii. In the case of an isothermal sphere, this leads to an underestimate of the mass by a factor of two. As a results, we estimate the mass of MS1008 within $1\,h_{50}^{-1}$ Mpc to be about $5.3 \times 10^{14}\,h_{50}^{-1}\,\mathrm{M}_\odot$.

3 Comparison with independent estimates

Since X-ray and redshifts data are available for this cluster, we can compare our mass determination with independent estimates. Lewis et al. (1999) estimated the mass within a radius $r \simeq 0.8\,h_{50}^{-1}$ Mpc from ROSAT HRI X-ray data and found $M_{\rm X} \simeq 3.6 \cdot 10^{14} h_{50}^{-1}\,\mathrm{M}_\odot$. This value is in excellent agreement with the lensing data provided that the mass sheet degeneracy is correctly taken into account (see before).

The analysis of the internal dynamics of MS1008, as traced by its member galaxies, has already been discussed in the literature by the CNOC collaboration. The internal (line-of-sight) velocity dispersion for this cluster was originally measured by Carlberg et al. (1996), who found $\sigma_v = (1054 \pm 107)$ km s^{-1}, based on the explicit background subtraction of the interloper con-

tamination. As a result, the virial estimate is slightly larger than the X-ray and lensing estimate. We stress however that the large errors in the virial, X-ray, and lensing estimates make all these determinations consistent to each other.

4 Conclusions

We have studied the weak lensing mass distribution of the cluster MS1008 using multicolor imaging data obtained during the Science Verification of FORS1 on the VLT and compared the results obtained with independent mass estimates.

We have found PSF distorsions of FORS1 to be moderate and hence easily removed with a low order polynomial fit. The B through I multicolor information, as well as the redshift information from the CNOC catalog, have allowed us to efficiently separate the background galaxies from the cluster and foreground populations. Approximately 3000 galaxies have been detected, and about 1700 have a good S/N and have been used for the determination of lensing shear field.

We have also compared the weak lensing mass profile with that derived from a virial analysis of the CNOC redshift data, as well as with the X-ray mass. The mass derived from X-ray observations (Lewis et al. 1999) is found in excellent agreement with our weak lensing determination at $r \simeq 0.8$ Mpc. The virial mass seems to be slightly larger than the mass obtained by our analysis, but given the errors this discrepancy is found to be not significant.

This analysis shows that the combination of depth and good imaging quality provided by VLT/FORS allows us to obtain high S/N mass maps via optimized weak lensing reconstruction methods. On the other hand, it also shows that systematic errors in weak lensing estimates can play a fundamental role. We find particularly problematic the mass sheet degeneracy, which must be removed by assuming a particular model for the mass distribution. This, clearly, can introduce some biases and makes weak lensing mass estimates (which in principle are "parameter free") model-depend.

1. Boehringer H., Tanaka Y., Mushotzky R.F., Ikebe Y., Hattori M., 1998, A&A 334, 789
2. Carlberg R.G., Yee H.K.C., Ellingson E., Abraham R., Gravel P., Morris S., Pritchet C.J., 1996, ApJ 462, 32
3. Fernández-Soto A., Lanzetta K.M, Yahil A., 1999, ApJ in press
4. Hoekstra H., Franx M., Kuijken K., Squires G., 1997, ApJ 504, 636
5. Kaiser N., Squires G., Broadhurst T., 1995, ApJ 449, 460
6. Lewis A.D., Ellingson E., Morris S.L., Carlberg R.G., 1999, ApJ 517, 587
7. Lombardi M., Bertin G., 1999, A&A 348, 38
8. Lombardi M., Rosati P., Nonino M., Girardi M., Borgani S., Squires G., 2000, in preparation
9. Luppino G.A., Kaiser N., 1997, ApJ 475, 20
10. Mellier Y., 1999, Annual Review of Astronomy and Astrophysiscs 37, 127
11. Schneider P., Seitz C., 1995, A&A 294, 411
12. Tyson J.A., Valdes F., Jarvis J.F., Mills A.P., 1984, ApJ 281, L59
13. Wu X.P., Fang L.Z., 1997, ApJ 483, 62
14. Yee H.K.C., Ellingson E., Morris S.L., Abraham R.G., Carlberg R.G., 1998, ApJS 116, 211